Supporting Information

All-solution-processed inorganic $CsPbBr_3$ solar cells and their bifacial-irradiation functions

Hiroaki Daiguji, Hiroto Takano, Ibuki Watanabe, Rin Ando, Manabu Ishizaki* and Masato Kurihara*

Faculty of Science, Yamagata University, 1-4-12 Kojirakawa-machi, Yamagata, Yamagata 990-8560, Japan.
Email: kurihara@sci.kj.yamagata-u.ac.jp; manabu-ishizaki@sci.kj.yamagata-u.ac.jp.

Table S1 Monofacial-irradiation photovoltaic parameter values of HTL-free $CsPbBr_3$ solar cells of FTO/TiO_2/$CsPbBr_3$/carbon using carbon pastes as top electrodes fabricated on commercial transparent FTO glass substrates as bottom electrodes

Refs.	Preparation method		J_{sc} (mA cm^{-2})	V_{oc} (V)	FF	PCE (%)	Irradiation area (cm^2)
	$CsPbBr_3$	top electrodes					
1	D	S	6.81	1.43	0.7996	7.81	0.06
2	D	S	6.49	1.42	0.79	7.22	0.16
*3	D	S	7.16	1.357	0.7297	7.09	0.09
4	D	S	9.55	1.413	0.73	9.86	0.09
5	D	S	7.11	1.372	0.7299	7.12	-
6	D	S	7.24	1.522	0.804	8.86	-
7	S/D	S	7.32	1.43	0.78	8.16	-
8	S	S	8.12	1.46	0.81	9.6	0.1
9	S	S	8.06	1.528	0.83	10.22	0.09
	S	S	7.84	1.397	0.75	8.21	1
10	S	S	7.47	1.36	0.68	6.91	0.09
11	S	S	5.99	1.33	0.657	5.25	-
12	S	S	7.03	1.40	0.75	7.52	0.8
13	S	S	7.48	1.19	0.688	6.12	0.04
14	S	S	7.56	1.52	0.827	9.53	0.09
15	S	S	7.12	1.49	0.6884	7.29	0.09
16	S	S	8.74	1.23	0.754	8.11	0.04
17	S	S	4.5	1.23	0.69	3.8	0.071
18	S	S	7.4	1.24	0.73	6.7	0.12
This work	S	S	7.49	1.48	0.79	8.68	0.049
			7.22	1.45	0.77	8.13	0.156

D; dry process. S; solution process. *The carbon electrode was formed using a carbon paste containing carbon nanotubes and MXene. All top carbon electrodes are opaque. In this study, the top SWNT electrode is semitransparent with a controlled transmittance value of 60%T at 550 nm. The photovoltaic parameter values are based on monofacial irradiation through FTO.

References

1. L. Liu, S.-E. Yang, P. Liu and Y. Chen, High-quality and full-coverage $CsPbBr_3$ thin films via electron beam evaporation with post-annealing treatment for all-inorganic perovskite solar cells, *Solar Energy*, 2022, **232**, 320–327.
2. J. Hua, X. Deng, C. Niu, F. Huang, Y. Peng, W. Li, Z. Ku and Y.-B. Cheng, A pressure-assisted annealing method for high quality $CsPbBr_3$ film deposited by sequential thermal evaporation, *RSC Adv.*, 2020, **10**, 8905–8909.
3. L. Mi, Y. Zhang, T. Chen, E. Xu and Y. Jiang, Carbon electrode engineering for high efficiency all-inorganic perovskite solar cells, *RSC Adv.*, 2020, **10**, 12298–12303.
4. G. Tong, T. Chen, H. Li, L. Qiu, Z. Liu, Y. Dang, W. Song, L. K. Ono, Y. Jiang and Y. Qi, Phase transition induced recrystallization and low surface potential barrier leading to 10.91%-efficient $CsPbBr_3$ perovskite solar cells, *Nano Energy*, 2019, **65**, 104015.
5. G. Tong, T. Chen, H. Li, W. Song, Y. Chang, J. Liu, L. Yu, J. Xu, Y. Qi and Y. Jiang, High efficient hole extraction and stable all-bromide inorganic perovskite solar cells via derivative-phase gradient bandgap architecture, *Sol. RRL*, 2019, **3**, 1900030.
6. Y. Zhang, L. Luo, J. Hua, C. Wang, F. Huang, J. Zhong, Y. Peng, Z. Ku and Y.-B. Cheng, Moisture assisted $CsPbBr_3$ film growth for high-efficiency, all-inorganic solar cells prepared by a multiple sequential vacuum deposition method, *Mater. Sci. Semicond. Process.*, 2019, **98**, 39–43.
7. X. Li, Y. Tan, H. Lai, S. Li, Y. Chen, S. Li, P. Xu and J. Yang, All-inorganic $CsPbBr_3$ perovskite solar cells with 10.45% efficiency by evaporation-assisted deposition and setting intermediate energy levels, *ACS Appl. Mater. Interfaces*, 2019, **11**, 29746–29752.

8. J. Yan, S. Hou, X. Li, J. Dong, L. Zou, M. Yang, J. Xing, H. Liu and H. Hao, Preparation of highly efficient and stable $CsPbBr_3$ perovskite solar cells based on an anti-solvent rinsing strategy, *Sol. Energy Mater. Sol. Cells*, 2022, **234**, 111420.
9. Z. Zhang, Y. Ba, D. Chen, J. Ma, W. Zhu, H. Xi, D. Chen, J. Zhang, C. Zhang and Y. Hao, Generic water-based spray-assisted growth for scalable high-efficiency carbon-electrode all-inorganic perovskite solar cells, *iScience*, 2021, **24**, 103365.
10. X. Han, X. Wang, J. Feng, H. Huang, Z. Zhu, T. Yu, Z. Li and Z. Zou, Carrier Mobility Enhancement in (121)-Oriented $CsPbBr_3$ Perovskite Films Induced by the Microstructure Tailoring of $PbBr_2$ Precursor Films, *ACS Appl. Electron. Mater.*, 2021, **3**, 373–384.
11. Li, Z. Zhu, X. Han, T. Yu, Y. Xu, J. Feng, Z. Li and Z. Zou, Direct Molecule Substitution Enabled Rapid Transformation of Wet $PbBr_2$(DMF) Precursor Films to $CsPbBr_3$ Perovskite, *ACS Appl. Energy Mater.*, 2021, **4**, 6414–6421.
12. S. Wang, W. Shen, Y. Chu, W. Zhang, L. Hong, A. Mei, Y. Rong, Y. Tang, Y. Hu and H. Han, Mesoporous-carbon-based fully-printable all-inorganic monoclinic $CsPbBr_3$ perovskite solar cells with ultrastability under high temperature and high humidity, *J. Phys. Chem. Lett.*, 2020, **11**, 9689–9695.
13. X. Cao, G. Zhang, L. Jiang, Y. Cai, Y. Gao, W. Yang, X. He, Q. Zeng, G. Xing, Y. Jia and J. Wei, Water, a green solvent for fabrication of high-quality $CsPbBr_3$ films for efficient solar cells, *ACS Appl. Mater. Interfaces*, 2020, **12**, 5925–5931.
14. Y. Wu, Y. Wang, J. Duan, X. Yang, J. Zhang, L. Liu and Q. Tang, Cluster effect of additives in precursors for inorganic perovskites solar cells, *Electrochim. Acta*, 2020, **331**, 135379.
15. Q. Meng, J. Feng, H. Huang, X. Han, Z. Zhu, T. Yu, Z. Li and Z. Zou, Simultaneous optimization of phase and morphology of $CsPbBr_3$ films via controllable Ostwald ripening by ethylene glycol monomethylether/isopropanol bi-solvent engineering, Adv. Eng. Mater., 2020, **22**, 2000162
16. X. Cao, G. Zhang, Y. Cai, L. Jiang, X. He, Q. Zeng, J. Wei, Y. Jia, G. Xing and W. Huang, All green solvents for fabrication of $CsPbBr_3$ films for efficient solar cells guided by the Hansen solubility theory, *Sol. RRL*, 2020, **4**, 2000008.
17. Z. Liu, B. Sun, X. Liu, J. Han, H. Ye, T. Shi, Z. Tang and G. Liao, Efficient carbon-based $CsPbBr_3$ inorganic perovskite solar cells by using Cu-phthalocyanine as hole transport material, *Nano-Micro Lett*, 2018, **10**, 34.
18. J. Liang, C. Wang, Y. Wang, Z. Xu, Z. Lu, Y. Ma, H. Zhu, Y. Hu, C. Xiao, X. Yi, G. Zhu, H. Lv, L. Ma, T. Chen, Z. Tie, Z. Jin and J. Liu, All-inorganic perovskite solar cells, *J. Am. Chem. Soc.*, 2016, **138**, 15829–15832.

Table S2 Monofacial-irradiation photovoltaic parameter values of see-through $CsPbBr_3$ solar cells fabricated on commercial transparent ITO or FTO glass substrates as bottom electrodes

Refs.	Cell configuration	Preparation method		J_{sc}	V_{oc} (V)	FF	PCE (%)	Irradiation area
		$CsPbBr_3$	top electrode	(mA cm^{-2})				(cm^2)
1	FTO/SnO_2/$CsPbBr_3$/NiO_x/ITO	D	D	6.67	1.55	0.70	7.28	0.4175
2	FTO/ZnO/$CsPbBr_3$/spiro-OMeTAD/ITO	S	D	3.73	0.94	0.3495	4.94	0.25
3	ITO/SnO_x/$CsPbBr_3$/P3HT/ITO nanoparticles/Ag nanowires	S	S	6.33	1.32	0.677	5.64	0.04
4	ITO/ZnO/$CsPbBr_3$/spiro-OMeTAD/PEDOT:PSS	D	S	6.15	1.38	0.7051	5.98	0.1
This work	FTO/TiO_2/$CsPbBr_3$/SWNT at 60%T	S	S	7.49 7.22	1.48 1.45	0.79 0.77	8.68 8.13	0.049 0.156

D; dry process. S; solution process. The top electrodes are (semi)transparent to prepare see-through $CsPbBr_3$ solar cells. The see-through solar cells (Refs. 2–4) include organic semiconductors of spiro-OMeTAD and P3HT as an HTL. The photovoltaic parameter values are based on monofacial irradiation through the bottom electrodes of FTO or ITO.

References

1. X. Jiang, C. Geng, X. Yu, J. Pan, H. Zheng, C. Liang, B. Li, F. Long, L. Han, Y.-B. Cheng and Y. Peng, Doping with KBr to achieve high-performance $CsPbBr_3$ semitransparent perovskite solar cells. *ACS Appl. Mater. Interfaces,* 2024, **16**, 19039−19047.
2. T. Das, R. Nag, N. K. Rana, M. Nayak, R. Paramanik, A. Bera, S. K. Saha and A. Guchhait, Effect of transition metal doping in the ZnO nanorod on the efficiency of the electron transport layer in semitransparent $CsPbBr_3$ perovskite solar cells. *Energy Fuels,* 2023, **37**, 10642−10651.
3. B. Parida , S. Yoon and D.-W. Kang, Room-temperature solution-processed 0D/1D bilayer electrodes for translucent $CsPbBr_3$ perovskite photovoltaics. *Nanomaterials*, 2021, **11**, 1489.
4. W. Chen, J. Zhang, G. Xu, R. Xue, Y. Li, Y. Zhou, J. Hou and Y. Li, A semitransparent inorganic perovskite film for overcoming ultraviolet light instability of organic solar cells and achieving 14.03% efficiency, *Adv. Mater.,* 2018, **30**, 1800855.

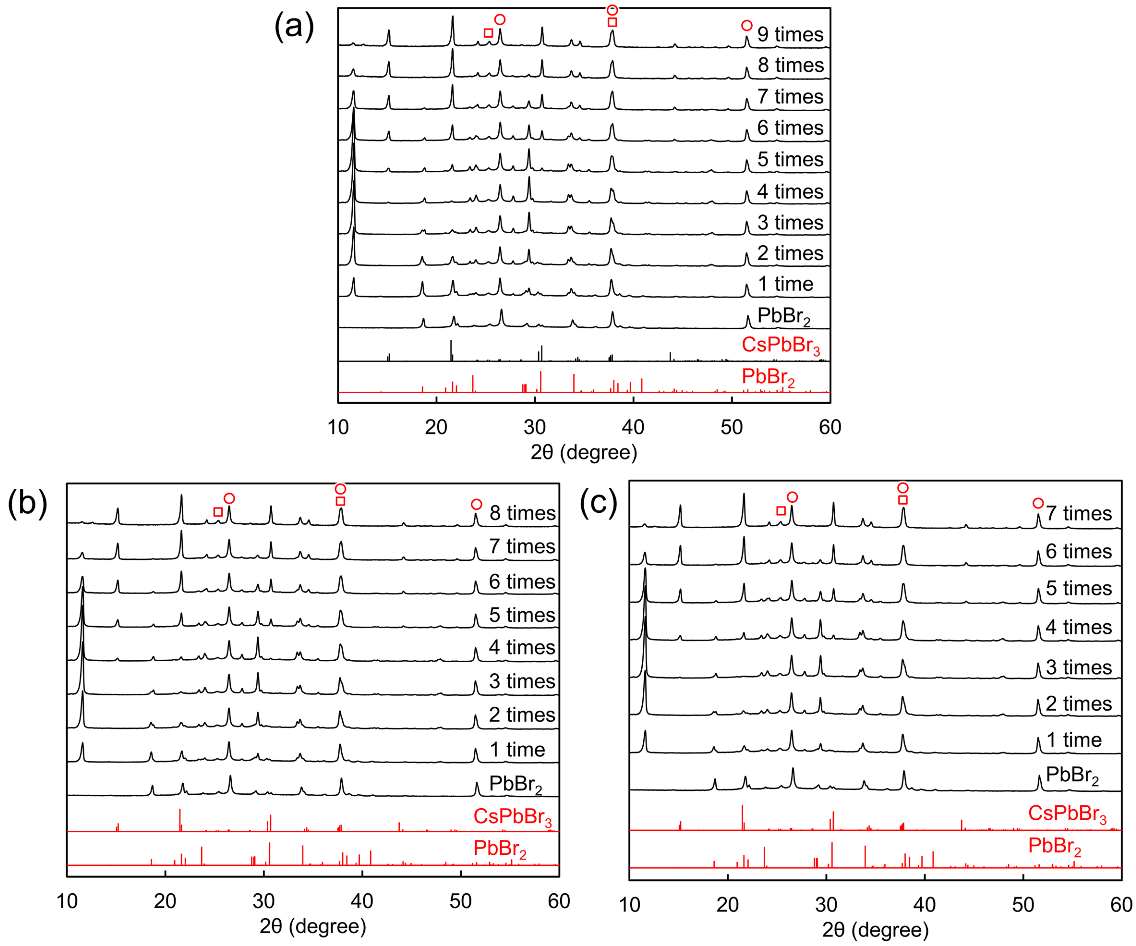

Fig. S1 Change in XRD patterns via a two-step spin-coating method to prepare $CsPbBr_3$ layers on mp-TiO_2/c-TiO_2/FTO using a $PbBr_2$ solution of (a) 1.40, (b) 1.30 or (c) 1.20 mol L^{-1}. The spin-coating with a CsBr solution was repeated 7 to 9 times on $PbBr_2$/mp-TiO_2/c-TiO_2/FTO until a strong signal at 11.6° of $CsPb_2Br_5$ almost disappeared. The signal positions of FTO (= SnO_2) and TiO_2 are indicated by □ and ○, respectively.

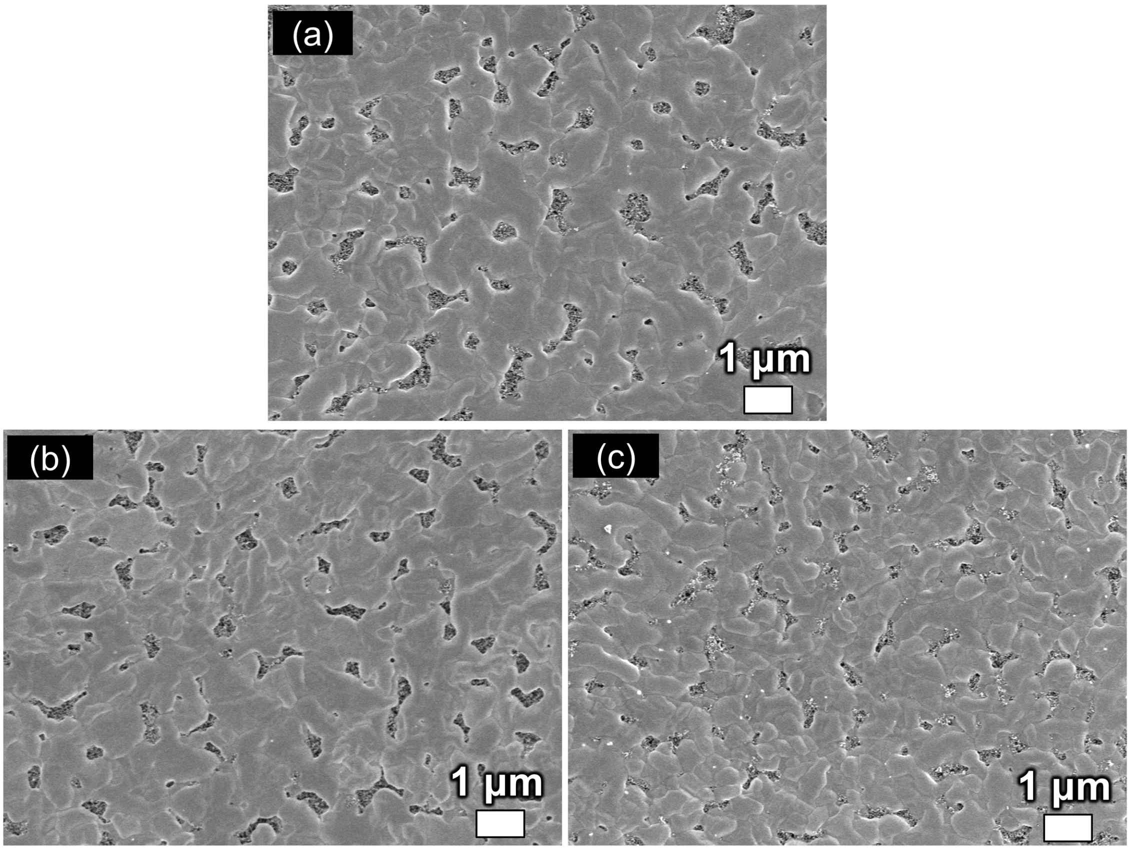

Fig. S2 Top-view FE-SEM images of $PbBr_2$ layers on mp-TiO_2/c-TiO_2/FTO using a $PbBr_2$ solution of (a) 1.40, (b) 1.30 or (c) 1.20 mol L^{-1}.

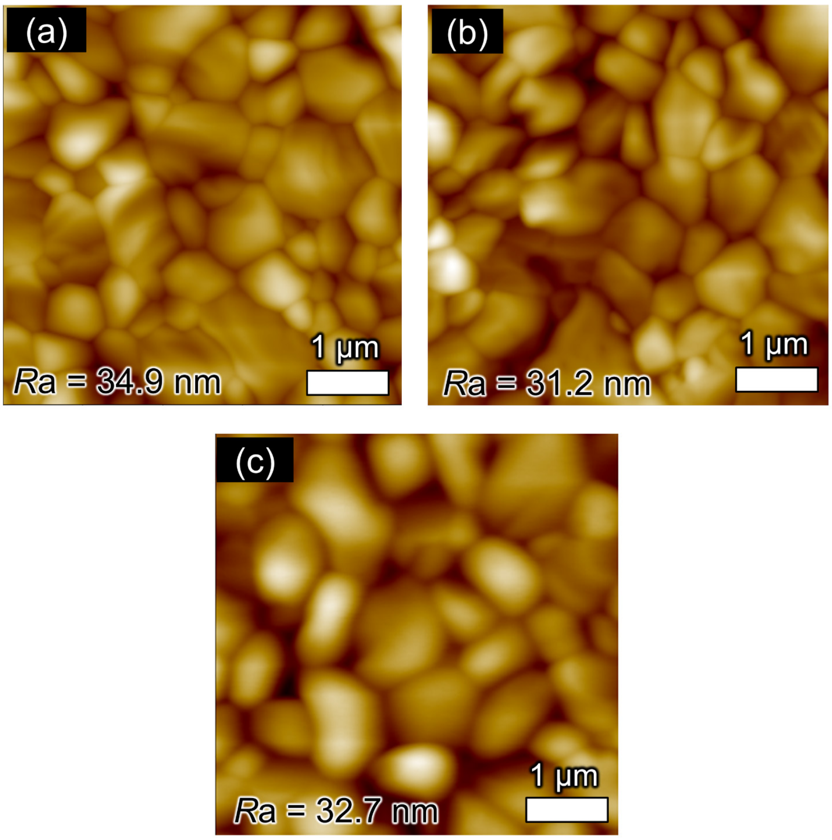

Fig. S3 AFM images of $CsPbBr_3$ grains on FTO/c-TiO_2/mp-TiO_2 using a $PbBr_2$ solution of (a) 1.20, (b) 1.30 or (c) 1.40 mol L^{-1}. *R*a values show average surface roughness.

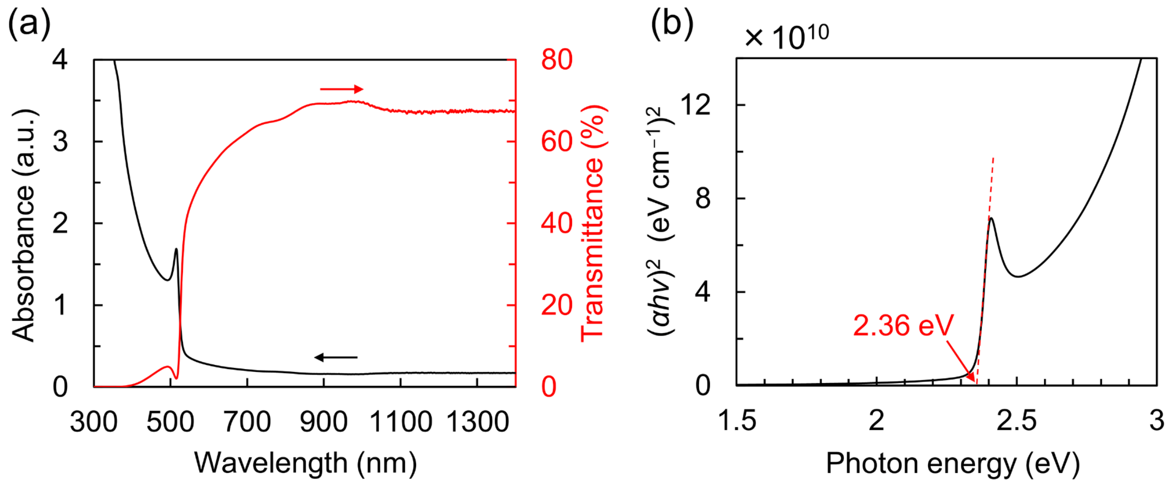

Fig. S4 (a) UV-Vis-near IR absorption/transmittance spectrum of FTO/c-TiO_2/mp-TiO_2/$CsPbBr_3$ (1.40 mol L^{-1}). A sharp absorption at 505 nm is characteristic of a direct-transition semiconductor. The bandgap energy (E_g) is estimated as 2.36 eV based on a Tauc plot (b) transformed from (a).

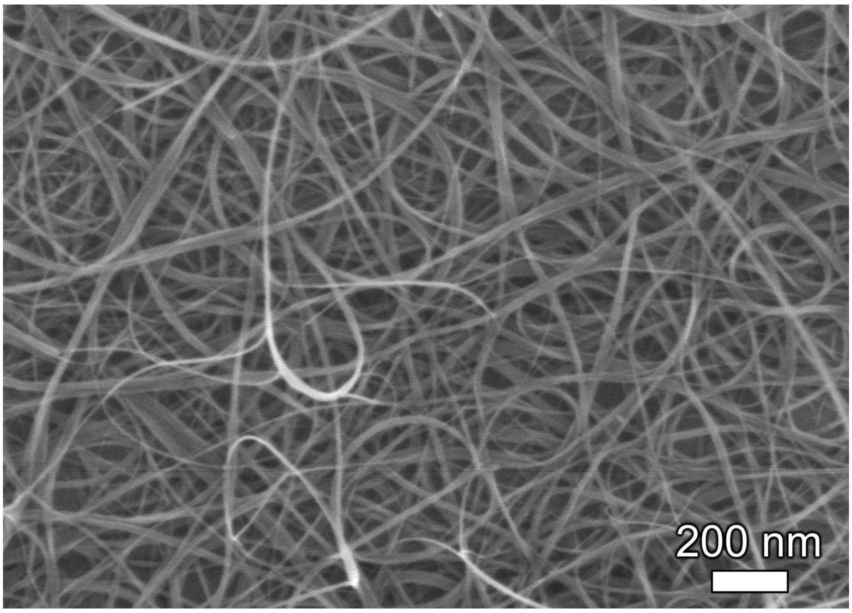

Fig. S5 Top-view SEM image of a SWNT thin film (60%T) transferred onto a glass substrate. Commercial SWNTs with a nominal diameter of 1.5 nm form bundles with an average width between 6 and 60 nm.

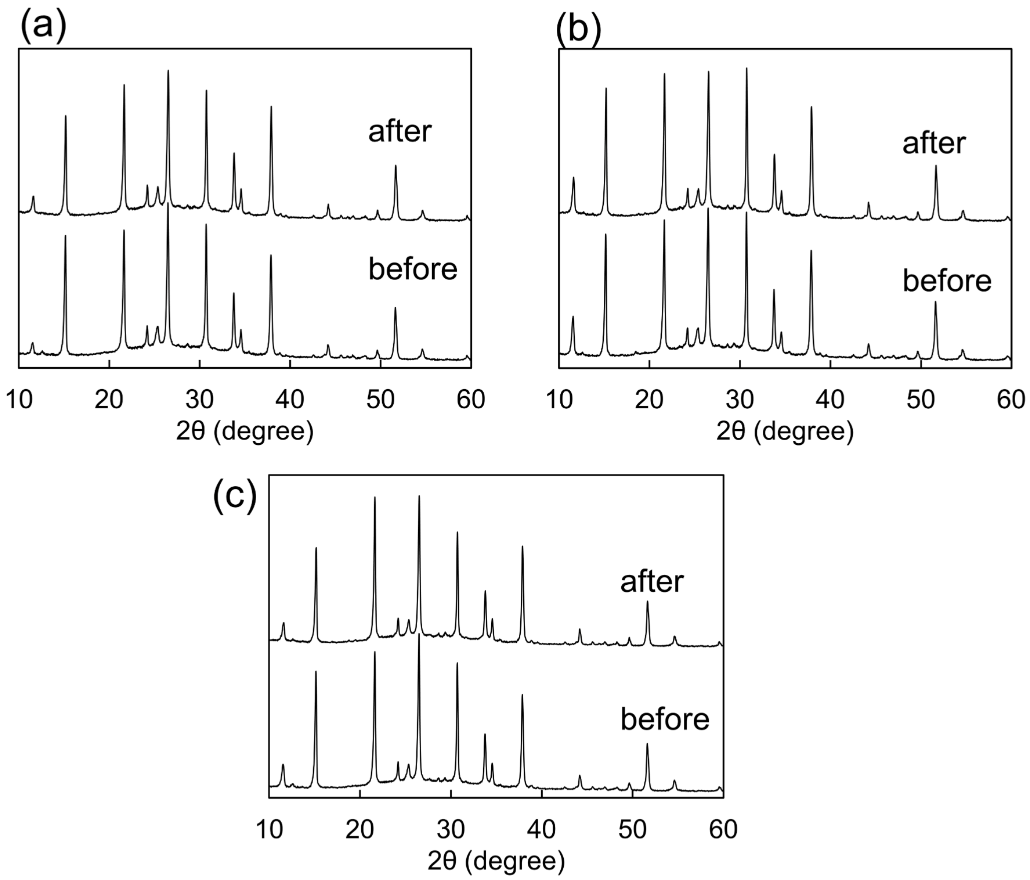

Fig. S6 XRD patterns of s-PSCs before/after transferring the semitransparent SWNT thin film. The $CsPbBr_3$ layer was prepared using a $PbBr_2$ solution of (a) 1.20, (b) 1.30 or (c) 1.40 mol L^{-1}.

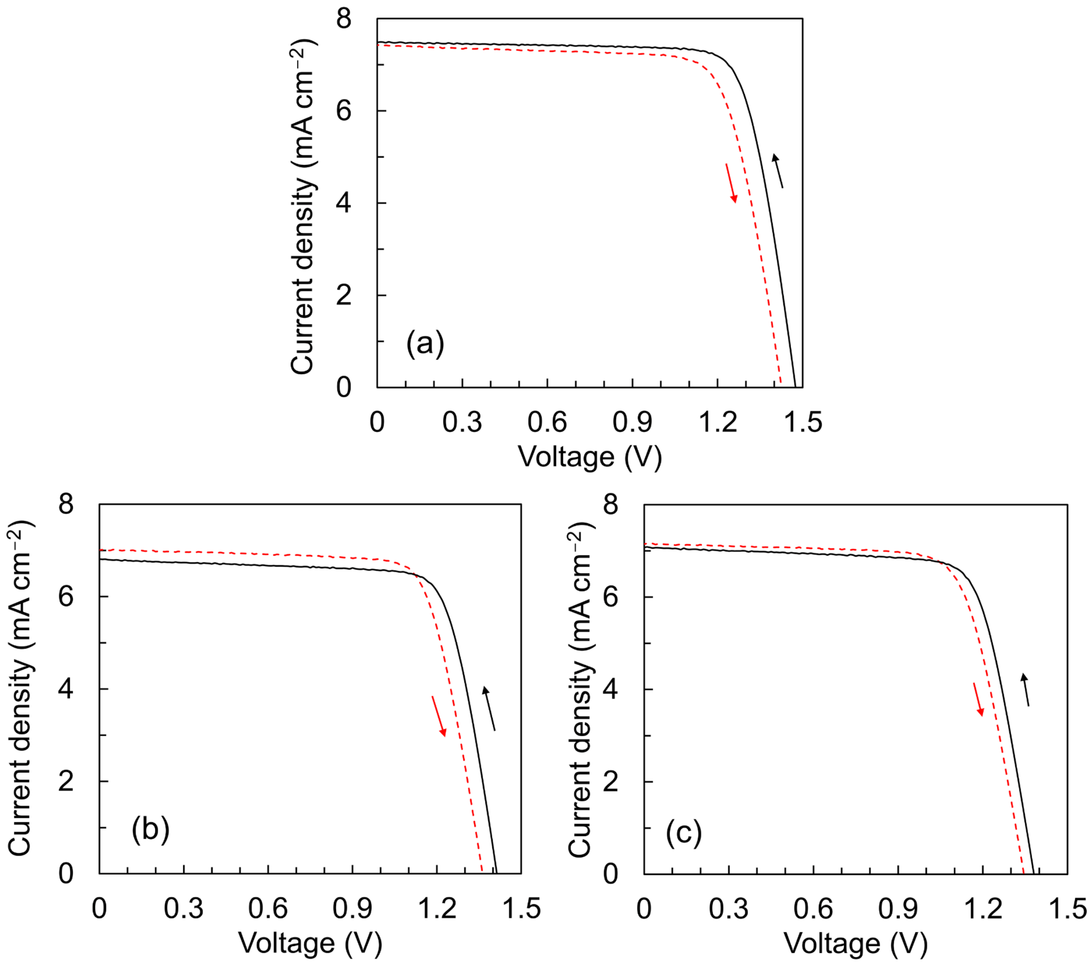

Fig. S7 *J-V* curves of s-PSCs at 60%T under monofacial irradiation using pseudo sunlight (100 mW cm^{-2}) through FTO at an area of 4.90 $\times 10^{-2}$ cm^2. The $CsPbBr_3$ layer was prepared using a $PbBr_2$ solution of (a) 1.40, (b) 1.30 or (c) 1.20 mol L^{-1}. Photovoltaic parameter values are summarized in the following table.

Table Photovoltaic parameter values based on Fig. S7

Concentration of $PbBr_2$ solutions (mol L^{-1})	Scan direction	J_{SC} (mA·cm^{-2})	V_{OC} (V)	FF	PCE (%)	HI (%)
1.2	forward	7.15	1.35	0.74	7.14	2.99
	reverse	7.08	1.38	0.75	7.36	
1.3	forward	7.01	1.36	0.76	7.28	1.75
	reverse	6.81	1.41	0.77	7.41	
1.4	forward	7.42	1.43	0.76	8.01	7.72
	reverse	7.49	1.48	0.79	8.68	

HI values show the hysteresis index calculated as $(PCE_{reverse} - PCE_{forward})/PCE_{reverse} \times 100$ (%).

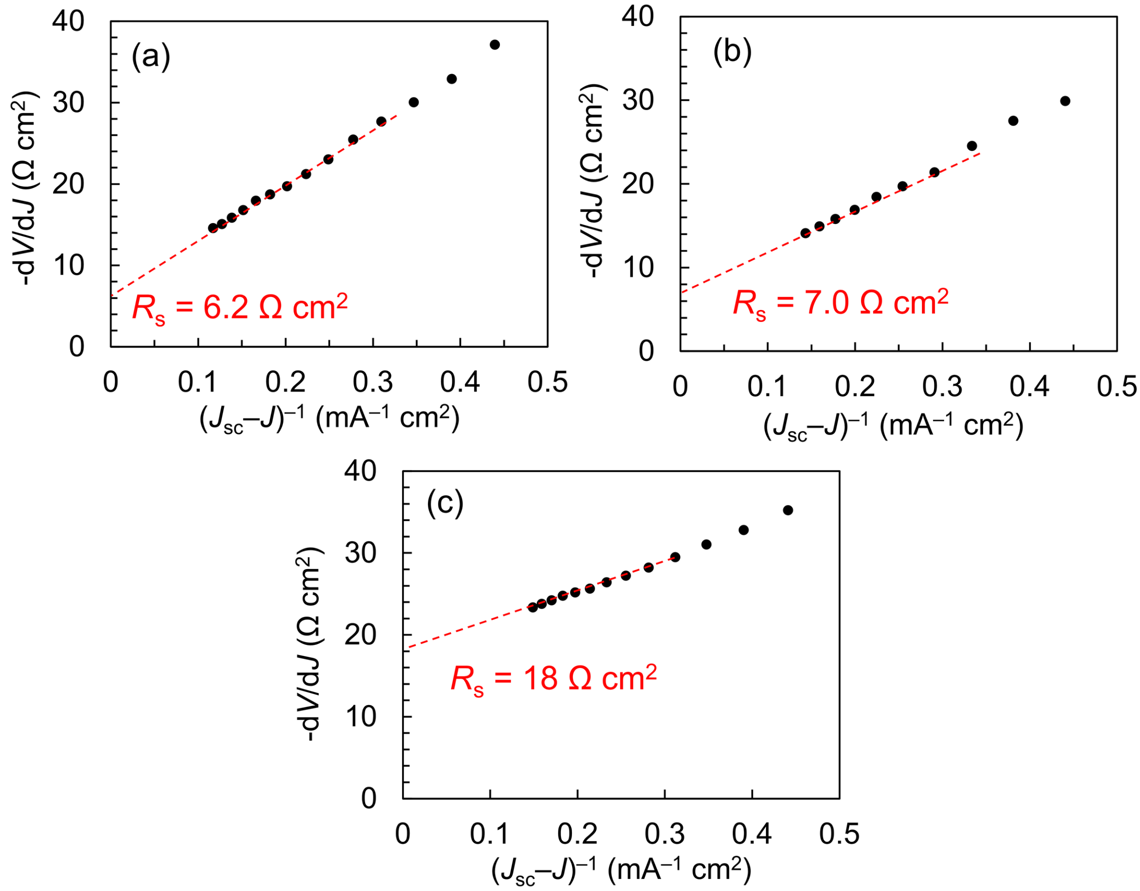

Fig. S8. Plots of -dV/dJ vs. $(J_{SC} - J)^{-1}$ and the linear fitting for calculation of series resistance (R_s) values. In a high-shunt-resistance (R_{sh}) condition, R_s values are estimated based on the following equation,[1,2]

$$-\frac{dV}{dJ} = \frac{mK_BT}{e}(J_{sc} - J)^{-1} + R_s$$

where V is the bias voltage, J is the current density, m is the ideality factor of a heterojunction, K_B is the Boltzman constant, T is the absolute temperature, e is the elementary charge, and J_{sc} is the short-circuit current density. R_s values are calculated from the linear-fitting intercepts using plots of -dV/dJ vs. $(J_{SC} - J)^{-1}$.

References

1. J. Shi, J. Dong, S. Lv, Y. Xu, L. Zhu, J. Xiao, X. Xu, H. Wu, D. Li, Y. Luo and Q. Meng, Hole-conductor-free perovskite organic lead iodide heterojunction thin-film solar cells: High efficiency and junction property, *Appl. Phys. Lett.*, 2014, **104**, 063901.
2. S. S. Hegedus and W. N. Shafarman, Thin-film solar cells: device measurements and analysis, *Prog. Photovoltaics Res. Appl.*, 2004, **12**, 155–176.

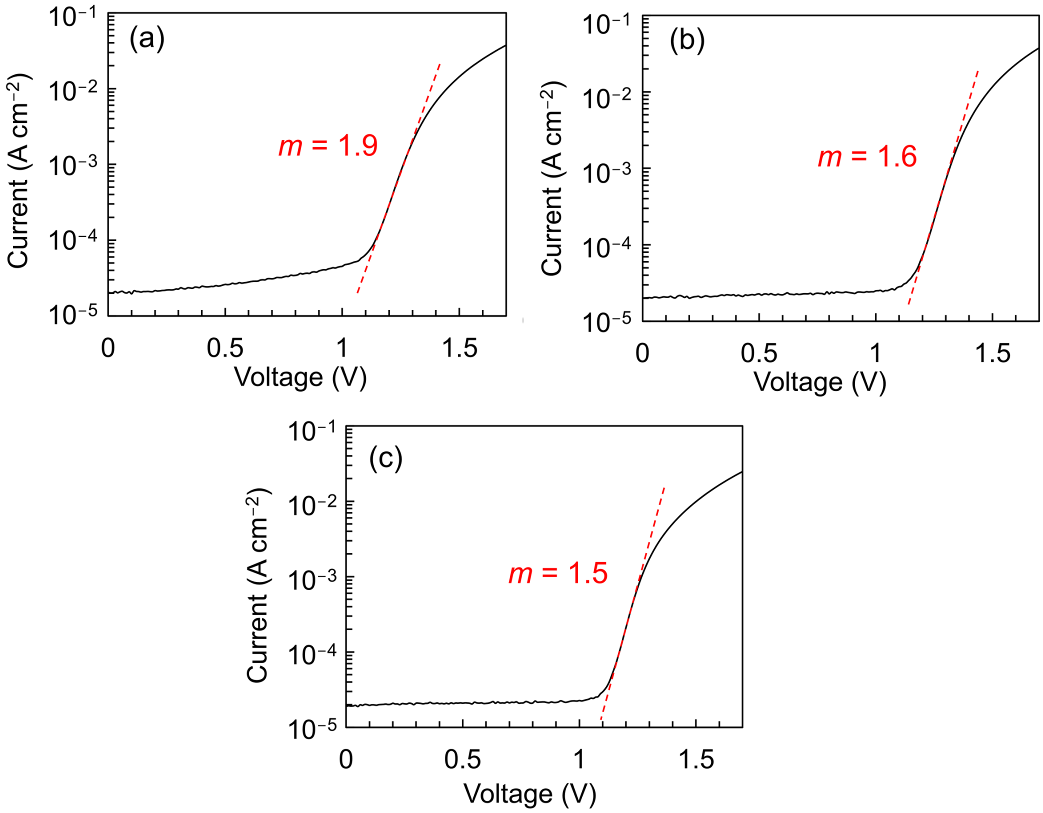

Fig. S9 *J*–*V* curves of s-PSCs at different transmittance values of (a) 60, (b) 70, and (c) 80%T in the dark. The *J*–*V* curves are composed of recombination currents in the diode space-charge region, diffusion currents, and diode diffusion currents limited by series resistance. Based on linearities (red dotted lines) of the diffusion currents versus applied voltages, the diode ideal factor (*m*) values were calculated between 1 and 2.

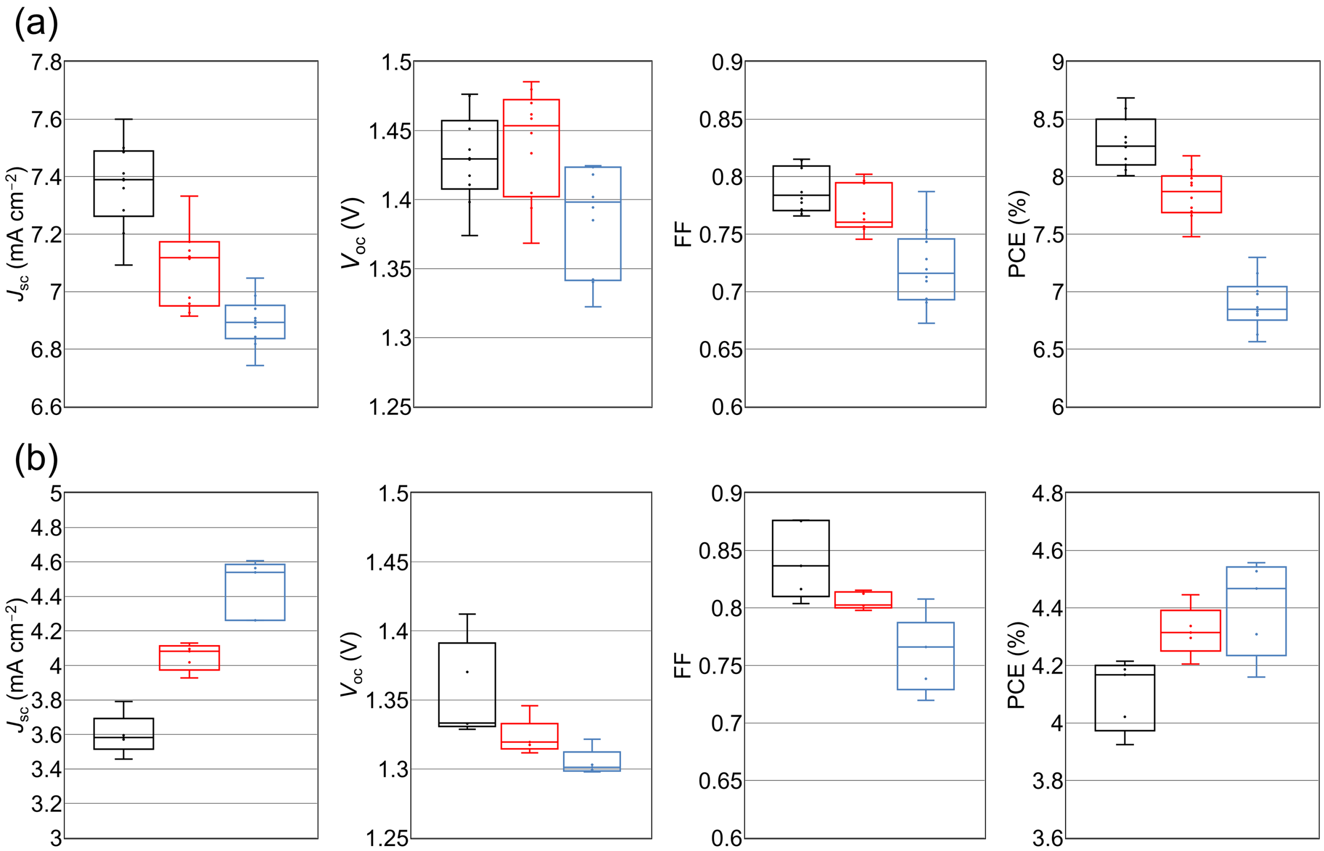

Fig. S10 Statistical distributions of the photovoltaic parameter values of s-PSCs at different transmittance values of 60 (black), 70 (red), and 80%T (blue) via the monofacial irradiation through (a) FTO and (b) SWNT.

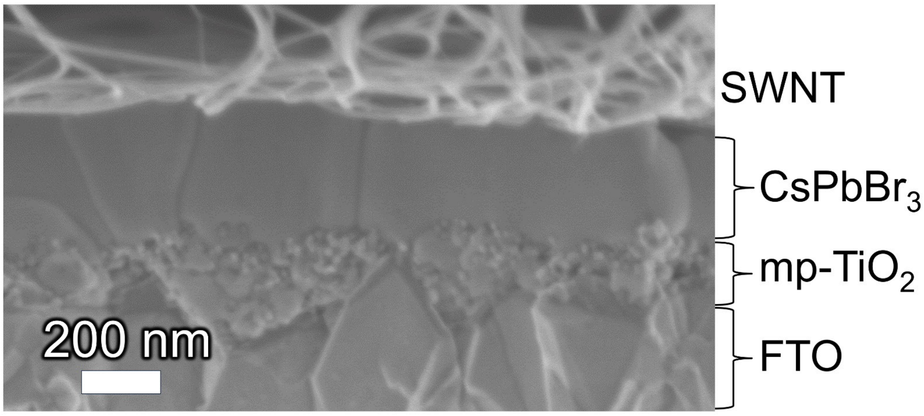

Fig. S11 Cross-sectional FE-SEM image of an s-PSC at 60%T. The SWNT bundles cannot penetrate the narrow spaces between monolayer-aligned large gains.

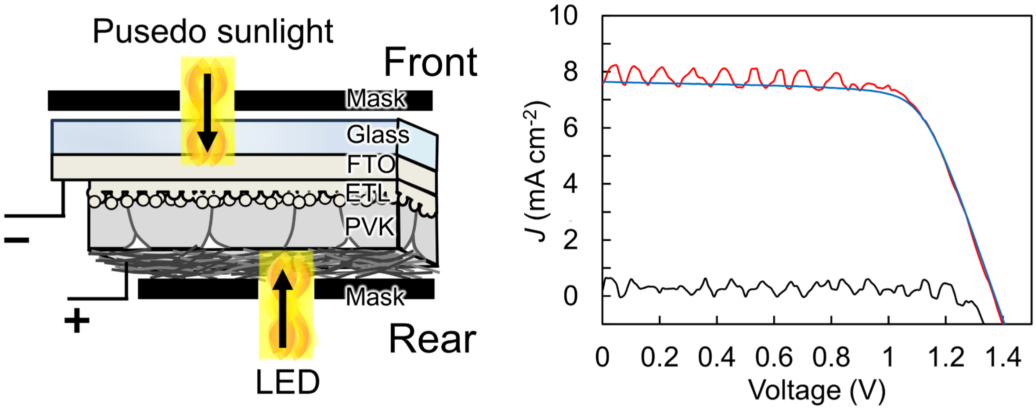

Fig. S12 *J-V* curves of an s-PSC at 60%T under monofacial irradiation using an on/off mode of LED light through SWNT (black line) and using pseudo sunlight (AM 1.5G) through FTO (blue line) and under bifacial irradiation using the on/off LED light through SWNT and pseudo sunlight through FTO (red line). As shown in the schematic PSC, the apertures (4.90×10^{-2} cm^2) for irradiation through the front (FTO) and rear (SWNT) electrodes are in different positions. The LED-light power ranges between 32% and 35% of the pseudo-sunlight power (100 mW cm^{-2}). The distance between the LED source and the PSC is adjusted to generate J_{sc} (SWNT) = 1.00 mA cm^{-2} in the case of 60%T. The *J-V* curve profile (red line) is nearly identical to Fig. 5b irradiated through the front (FTO) and rear (SWNT) electrodes at the same position.

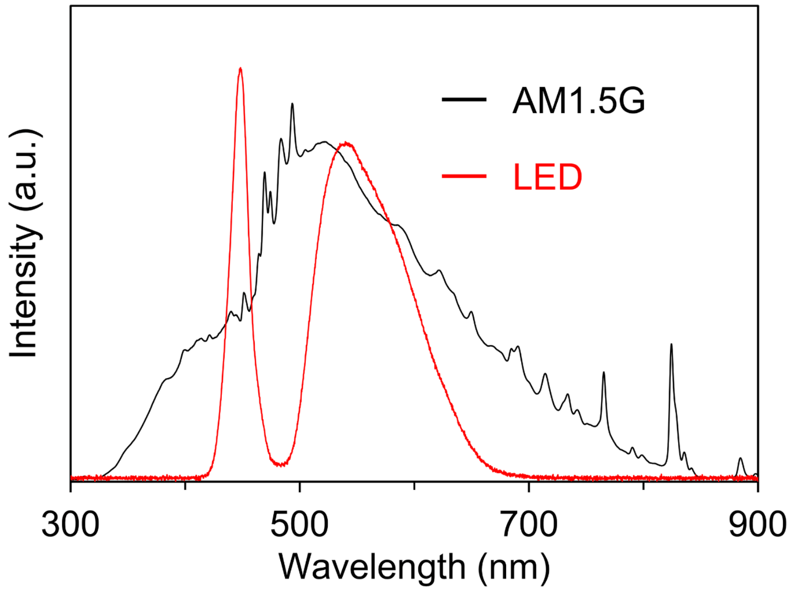

Fig. S13 Emission spectrum of the LED compared to the pseudo sunlight (AM 1.5G).

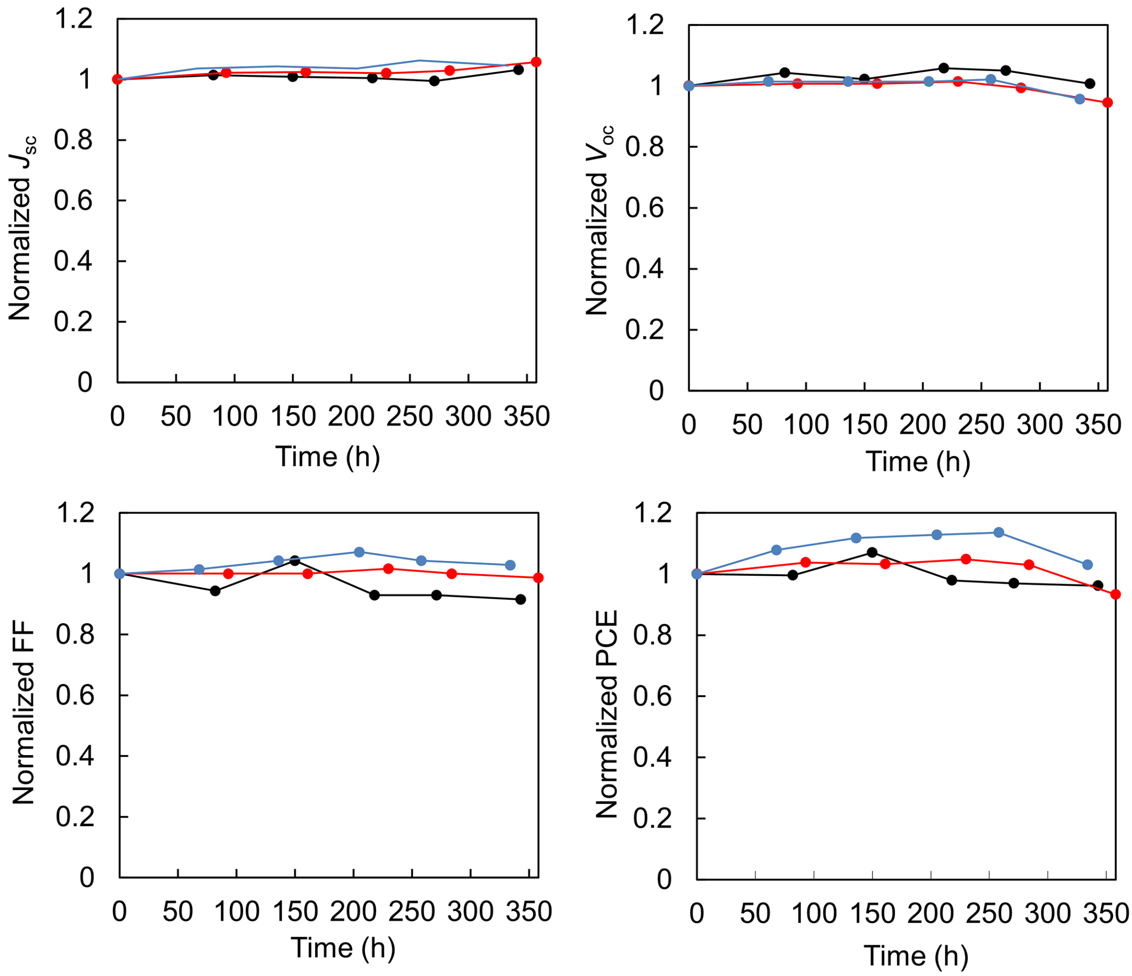

Fig. S14 Stability experiment of an s-PSC at 60%T exposure to ambient air without sealing.

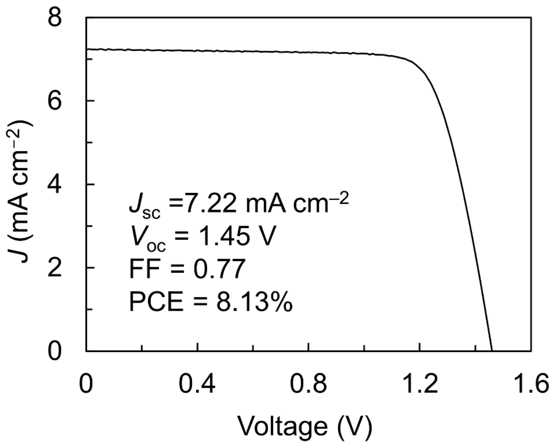

Fig. S15 *J-V* curve of an s-PSC at 60%T under monofacial irradiation using pseudo sunlight through FTO. The irradiation area is expanded to 1.56×10^{-1} from 4.90×10^{-2} cm^2 of Fig. 4a.